

Article

# Investigation of Dynamic Recrystallization of NiTi Shape Memory Alloy Subjected to Local Canning Compression

Yanqiu Zhang <sup>1</sup>, Shuyong Jiang <sup>1,\*</sup> and Li Hu <sup>2</sup>

<sup>1</sup> College of Mechanical and Electrical Engineering, Harbin Engineering University, Harbin 150001, China; zhangyq@hrbeu.edu.cn

<sup>2</sup> College of Materials Science and Chemical Engineering, Harbin Engineering University, Harbin 150001, China; heu\_huli@126.com

\* Correspondence: jiangshuyong@hrbeu.edu.cn; Tel.: +86-451-82519710

Academic Editor: Takuo Sakon

Received: 28 April 2017; Accepted: 1 June 2017; Published: 6 June 2017

**Abstract:** Physical mechanism for dynamic recrystallization of NiTi shape memory alloy subjected to local canning compression at various temperatures, 600, 700 and 800 °C, was investigated via electron backscattered diffraction experiments and transmission electron microscopy observations. With increasing deformation temperature, fractions of recrystallized grains and substructures increase, whereas fraction of deformed grains decreases. In the case of 600 and 700 °C, continuous dynamic recrystallization and discontinuous dynamic recrystallization coexist in NiTi shape memory alloy. In the case of discontinuous dynamic recrystallization, the recrystallized grains are found to be nucleated at grain boundaries and even in grain interior. The pile-up of statistically stored dislocation lays the foundation for the nucleation of the recrystallized grains during discontinuous dynamic recrystallization of NiTi shape memory alloy. Geometrically necessary dislocation plays as an important role in the formation of new recrystallized grains during continuous dynamic recrystallization of NiTi shape memory alloy.

**Keywords:** shape memory alloy; NiTi alloy; plastic deformation; dynamic recrystallization; microstructure

## 1. Introduction

NiTi-based shape memory alloys (SMAs) have been widely used in the engineering fields because they possess shape memory effect as well as superelasticity [1,2]. It is well known that plastic deformation at high temperatures is of great importance in manufacturing the products of NiTi-based SMAs [3–5]. In particular, dynamic recrystallization (DRX) frequently occurs during plastic deformation of NiTi-based SMAs at high temperatures [6–9]. It can be generally accepted that DRX has an influence on the microstructures of metallic alloys, which further have an effect on the mechanical properties [10,11]. As a consequence, it is important to investigate the DRX mechanisms of metallic alloys subjected to plastic deformation at high temperatures. In recent years, many researchers have devoted themselves to investigating the DRX of various metals subjected to uniaxial compression at high temperatures [12–17]. However, only a few literatures related to the DRX of NiTi-based SMAs have been reported. Yin et al. studied the mechanisms of DRX in the 50Ti-47Ni-3Fe SMA by means of uniaxial compression tests at the temperatures ranging from 750 to 1050 °C and at the strain rates ranging from 0.01 to 10 s<sup>-1</sup>, where continuous dynamic recrystallization (CDRX) was found [6]. Basu et al. investigated the DRX in an Ni-Ti-Fe SMA subjected to uniaxial compression at the temperatures of 750, 850 and 950 °C, respectively, and they found that the DRX is able to suppress calorimetric signatures of phase transformations from austenite to martensite [7]. Mirzadeh and Parsa

investigated hot compression behavior of 50.5 at % Ni–49.5 at % Ti SMA via flow stress curves at the temperatures ranging from 700 to 1000 °C and at the strain rate of  $0.1 \text{ s}^{-1}$ , where the typical single-peak DRX behavior was observed [9].

All the aforementioned investigations related to the DRX of NiTi-based SMAs were performed in the case of uniaxial compression at the temperatures above 700 °C. In addition, none of them focused on the mechanism of DRX in NiTi-based SMAs. In fact, the DRX may occur in the NiTi-based SMA which is deformed at a lower temperature of 600 °C [8]. It is well known that the deformation temperature is able to influence the mechanism of DRX. Furthermore, local canning compression may result in a different DRX behavior since it is able to provide a three-dimensional compression stress for the deformed materials. As a consequence, in the present work, a binary NiTi SMA was subjected to local canning compression at three temperatures (600, 700 and 800 °C) so as to investigate the physical mechanism of DRX.

## 2. Materials and Methods

### 2.1. Local Canning Compression

Commercially hot-rolled binary NiTi SMA bar with the composition of Ni<sub>50.9</sub>Ti<sub>49.1</sub> (at %) and the diameter of 12 mm was used as raw material. The NiTi SMA bar was provided by Xi'an saite metal materials development Co., Ltd., Xi'an, China. The NiTi SMA samples, whose diameter and height are 4 and 6 mm, respectively, were removed from the as-rolled NiTi SMA bar along the axial direction via an electro-discharge machining (EDM) (DK7725, Jiangsu Dongqing CNC Machine Tool Co., Ltd., Taizhou, China). Subsequently, they were locally canned by the cans made of low carbon steel. Therein, the inner diameter, outer diameter and the height of the cans are 4, 10 and 3 mm, respectively. Afterward, the local canning compression experiments were carried out on the INSTRON 5500 equipment (Instron Corporation, Norwood, MA, USA) at the strain rate of  $0.05 \text{ s}^{-1}$  and at 600, 700 and 800 °C, respectively. Furthermore, all the canned NiTi SMA samples were compressed by 75% in height. Subsequently, all the compressed NiTi SMA samples were quenched into water at room temperature. Finally, the compressed NiTi SMA samples were removed from the steel cans.

### 2.2. Materials Characterization

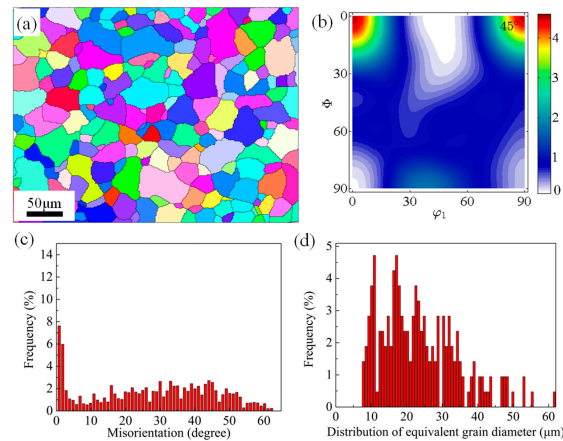
The samples for electron backscattered diffraction (EBSD) measurements were prepared based on the cross section which is parallel to axial direction of the as-rolled NiTi SMA bar as well as the compressed NiTi SMA samples. The NiTi SMA samples for EBSD observation were mechanically polished and subsequently electropolished in a solution, which is composed of 30% HNO<sub>3</sub> and 70% CH<sub>3</sub>OH by volume fraction, at –30 °C. EBSD experiments were performed on the NiTi SMA samples via Zeiss ULTRA plus scanning electron microscope (SEM) (University of South Carolina, Columbia, SC, USA), which is equipped with Oxford Instruments AZtec integrated energy-dispersive spectroscopy (EDS) and EBSD system. Microstructures of the compressed NiTi SMA samples were characterized via transmission electron microscopy (TEM). Foils for TEM observation were mechanically ground to 70 μm and then thinned by twin-jet polishing in an electrolyte which is composed of 6% HClO<sub>4</sub>, 34% C<sub>4</sub>H<sub>10</sub>O and 60% CH<sub>3</sub>OH by volume fraction. TEM observations were carried out on a FEI TECNAI G2 F30 microscope (FEI Corporation, Hillsboro, OR, USA), which possesses a side-entry and double-tilt specimen stage with angular range of ±40° at an accelerating voltage of 300 kV.

## 3. Results

### 3.1. EBSD Analysis of Microstructural Evolution

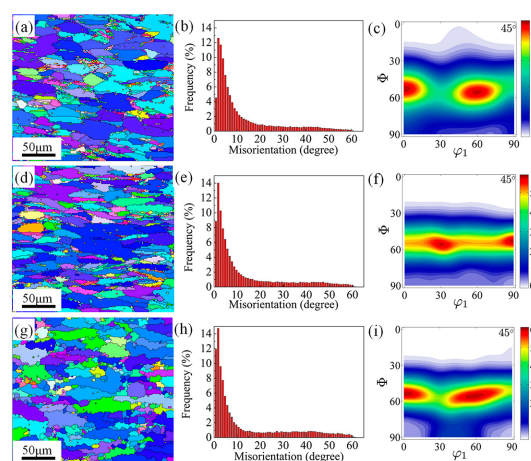
Based on EBSD experiment, the microstructure of the as-rolled NiTi SMA bar was characterized, and the corresponding results were shown in Figure 1. It can be seen from Figure 1 that the grains of

the as-rolled NiTi SMA bar exhibit a certain preferential orientation, where  $\langle 110 \rangle$  texture is dominant according to orientation distribution function (ODF). In addition, it can be found that the misorientation of the grains basically follows a normal distribution except that the grains with the misorientation of  $1\text{--}2^\circ$  exhibit a higher frequency, as shown in Figure 1c. In addition, it can be noted from Figure 1d that the size of grains mainly ranges from 10 to 60  $\mu\text{m}$ .



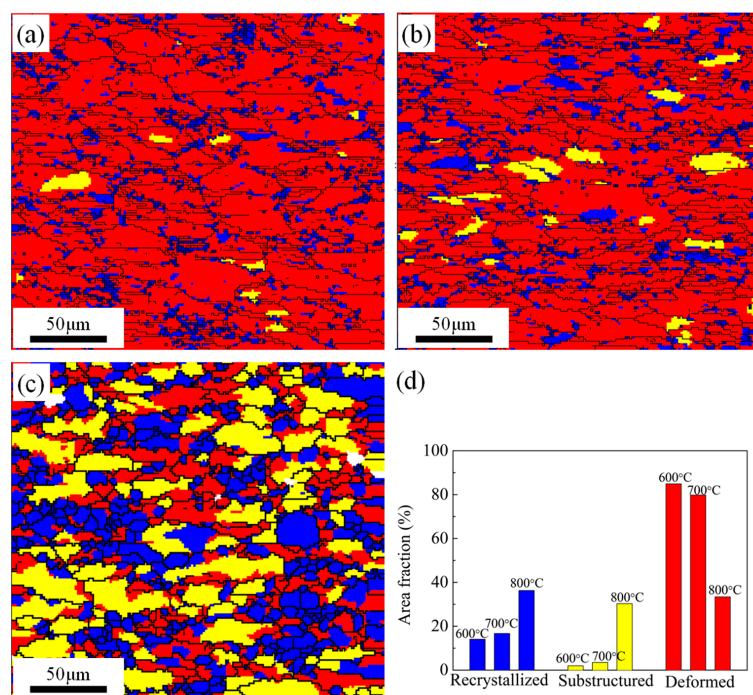
**Figure 1.** Microstructure characterization of as-rolled NiTi shape memory alloy (SMA) based on electron backscattered diffraction (EBSD) experiment: (a) distribution of grains with various orientations; (b) orientation distribution function (ODF); (c) misorientation angle distribution; (d) distribution of equivalent grain diameter.

Figure 2 shows the EBSD results of NiTi SMA subjected to canning compression at various temperatures, 600, 700 and 800  $^\circ\text{C}$ . It can be observed from Figure 2 that as compared to the as-rolled NiTi SMA, the grains with low angle grain boundaries are dominant in the compressed NiTi SMA. In particular,  $\langle 110 \rangle$  texture of the as-rolled NiTi SMA is transformed into  $\langle 111 \rangle$  texture of the compressed NiTi SMA as a result of plastic deformation. Furthermore, the intensity of  $\langle 111 \rangle$  texture increases with increasing deformation temperature. The aforementioned results indicate that DRX seems to have a significant influence on the texture evolution of NiTi SMA.



**Figure 2.** EBSD analysis of NiTi SMA subjected to local canning compression at various temperatures: (a) orientation map at 600  $^\circ\text{C}$ ; (b) misorientation distribution at 600  $^\circ\text{C}$ ; (c) ODF at 600  $^\circ\text{C}$ ; (d) Orientation map at 700  $^\circ\text{C}$ ; (e) misorientation distribution at 700  $^\circ\text{C}$ ; (f) ODF at 700  $^\circ\text{C}$ ; (g) orientation map at 800  $^\circ\text{C}$ ; (h) misorientation distribution at 800  $^\circ\text{C}$ ; (i) ODF at 800  $^\circ\text{C}$ .

For the purpose of further understanding DRX mechanisms of NiTi SMA, microstructures of NiTi SMA subjected to local canning compression at the various temperatures were characterized by means of EBSD experiment, as shown in Figure 3. The fractions of the recrystallized grains, the substructures and the deformed grains are captured in NiTi SMA subjected to local canning compression at 600, 700 and 800 °C. It can be noted that with increasing deformation temperature, the fractions of the recrystallized grains and the substructures increase, whereas the fraction of the deformed grains decreases. In fact, the three structures do not show such a considerable discrepancy between 600 and 700 °C. However, as compared to 600 and 700 °C, the three structures present an apparent discrepancy in NiTi SMA subjected to local canning compression at 800 °C. The aforementioned phenomena are attributed to the fact that dynamic recovery (DRV) and DRX are dominant in NiTi SMA subjected to local canning compression at 600 and 700 °C, while only DRX is dominant in NiTi SMA subjected to local canning compression at 800 °C.



**Figure 3.** EBSD analysis of dynamic recrystallized microstructures in NiTi SMA subjected to local canning compression at various temperatures: (a) DRX map at 600 °C; (b) DRX map at 700 °C; (c) DRX map at 800 °C; (d) Area fraction distribution of various microstructures. (The grains with the misorientation equal to or larger than 10° was defined as the recrystallized structures, and the grains with the misorientation ranging from 3 to 10° were regarded as the substructured structures, while the grains with the misorientation equal to or lower than 3° was identified as the deformed structures.)

Figure 4 shows a distribution of geometrically necessary dislocation (GND) density of NiTi SMA samples based on EBSD experiments. It can be observed that as compared to the as-rolled NiTi SMA sample, GND density shows little difference in the NiTi SMA samples subjected to local canning compression at 600, 700 and 800 °C. In addition, the deformation temperatures have little influence on GND density of NiTi SMA samples. Furthermore, as is expected, GND is mainly distributed at the grain boundaries.

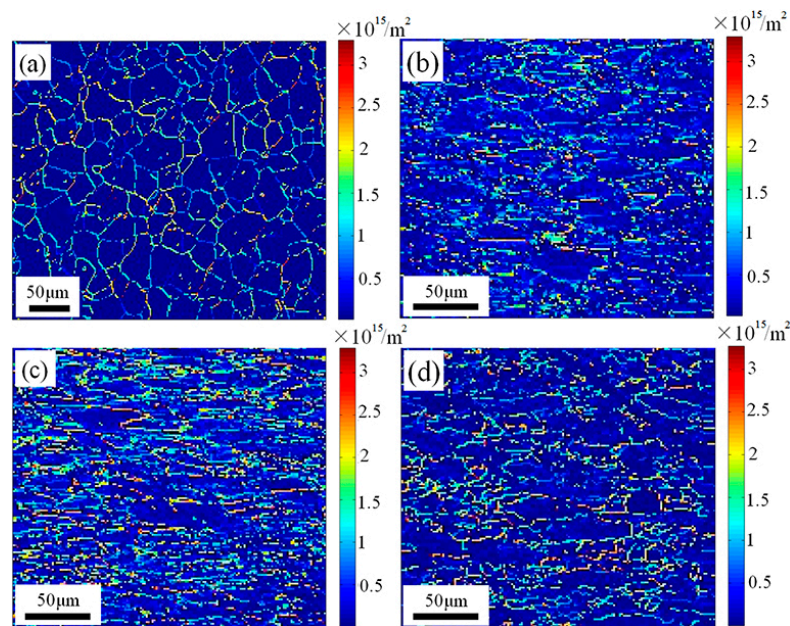


**Figure 4.** Distribution of geometrically necessary dislocation (GND) density in NiTi SMA subjected to local canning compression at various temperatures: (a) As-rolled; (b) 600 °C; (c) 700 °C; (d) 800 °C.

### 3.2. TEM Observation of Microstructural Evolution

TEM micrographs of NiTi SMA subjected to local canning compression at 600, 700 and 800 °C are shown in Figures 5–7, respectively, so that the corresponding mechanisms of DRX are further clarified. It can be found from Figure 5a that in the case of 600 °C, a high density of dislocations is distributed in the matrix of NiTi SMA with B2 austenite phase. In addition, the subgrain with low angle grain boundary can be observed in Figure 5c, where plenty of dislocations are distributed in the subgrain interior. In particular, the recrystallized grains can be observed in the grain interior in Figure 5d. However, as for NiTi SMA subjected to local canning compression at 700 °C, dislocation density is obviously reduced, as shown in Figure 6a. The recrystallized grain can be observed in the grain interior, as shown in Figure 6c, where plenty of dislocations are distributed in the recrystallized grain. Moreover, a triple-junction grain boundary can be observed in Figure 6d, where a few dislocations are distributed near the grain boundary. In particular, no recrystallized grain can be seen in the grain interior. However, when NiTi SMA is subjected to local canning compression at 800 °C, dislocation density is substantially reduced, as shown in Figure 7a. It is very difficult to capture the whole recrystallized grain as well as the subgrain by means of TEM observation. It can be observed that the parallel dislocation array is distributed near the grain boundary due to the pile-up of dislocations at the grain boundary.

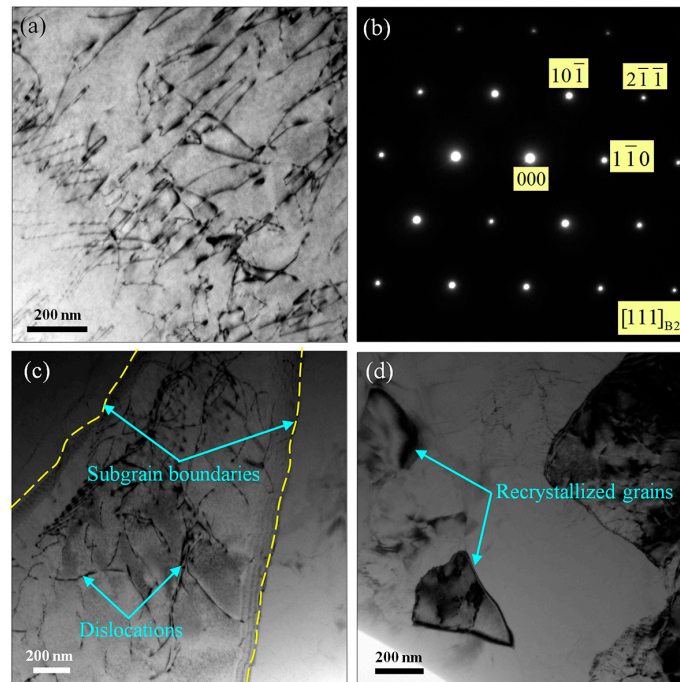


**Figure 5.** TEM micrographs of NiTi SMA subjected to local canning compression at 600 °C: (a) bright field image showing a high density of dislocations; (b) diffraction patterns of (a) showing the existence of B2 austenite; (c) bright field image showing the existence of subgrain boundary; (d) bright field image showing the existence of recrystallized grains.

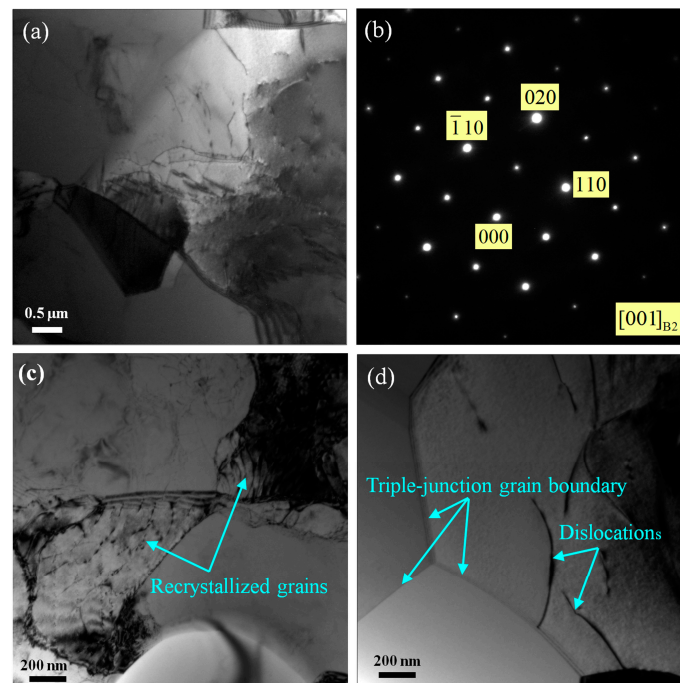


**Figure 6.** TEM micrographs of NiTi SMA subjected to local canning compression at 700 °C: (a) Bright field image; (b) diffraction patterns of (a) showing the existence of B2 austenite; (c) bright field image showing the formation of recrystallized grains at the grain boundary; (d) bright field image showing the existence of triple-junction grain boundary.

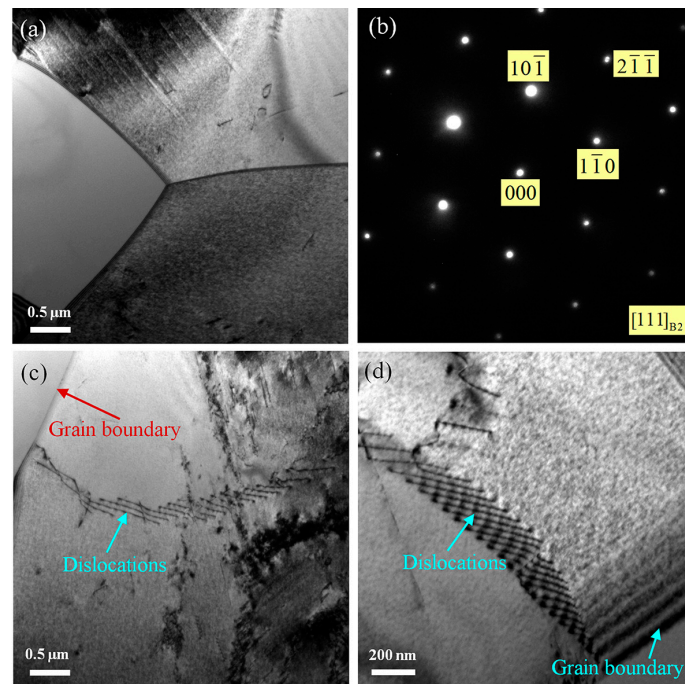


**Figure 7.** TEM micrographs of NiTi SMA subjected to local canning compression at 800 °C: (a) bright field image showing the existence of triple-junction grain boundary; (b) diffraction patterns of (a) showing the existence of B2 austenite; (c) bright field image showing the pile-up of dislocations at the grain boundary; (d) bright field image showing the existence of substructures due to parallel dislocations.

#### 4. Discussion

It is well known that DRX frequently occurs in the metal materials subjected to hot working. Consequently, the new grains, which are completely different from the original ones, arise in the initial microstructures. Furthermore, the factors, which have an influence on DRX, deal with deformation temperature, plastic strain, strain rate and nature of metal materials. So far as the latter is concerned, stacking fault energy is related closely to DRX of metal materials. In particular, it is generally accepted that DRX can be divided into discontinuous dynamic recrystallization (DDRX) and CDRX. In the case of DDRX, the formation of the recrystallized grains deals with the nucleation and the growth of new grains. In other words, DDRX has a characteristic of repeated nucleation and finite growth. However, in terms of CDRX, subgrain structures with low angle grain boundary are induced at the primary stage of plastic deformation and they are progressively transformed into the new grains with high angle grain boundaries after experiencing large plastic strain. In general, DDRX takes place in the metal materials with low to medium stacking fault energy at high temperatures more than  $0.5T_m$ , where  $T_m$  is the melting point of the metal materials. The melting point of the NiTi SMA used in the present study is determined as 1300 °C or so. CDRX is found to occur in all the metal materials regardless of their stacking fault energy when the deformation temperature is above  $0.5T_m$  and the metal materials are subjected to severe plastic deformation. However, at high temperatures above  $0.5T_m$ , CDRX are frequently observed in the metal materials with high stacking fault energy [10,11].

It is well known that dislocation density plays an important role in DRX of metals. In the case of DDRX, in particular, dislocation density shall become a driving force that facilitates the nucleation of new recrystallized grains during plastic deformation. In general, the new recrystallized grains are free of dislocations during DDRX. However, in the case of CDRX, the dislocations are progressively absorbed during transformation from low angle grain boundaries to high angle grain boundaries. Furthermore, CDRX frequently occurs along with DRV. Consequently, the dislocations can be frequently

observed in the recrystallized grains based on CDRX. According to the aforementioned analysis, it can be deduced that in the present study, DDRX and CDRX coexist during plastic deformation of NiTi SMA at 600 and 700 °C. It has been reported in the literatures that stacking fault energy is not a rigorous factor distinguishing between DDRX and CDRX since DDRX is observed in the metals with high stacking fault energy [18], while CDRX is observed in the metals with low stacking fault energy [19]. It can be generally accepted that DDRX frequently occurs in NiTi-based SMA [6–8]. However, recent literature has shown that CDRX is captured in NiTiFe SMA [9]. However, it seems that DDRX is dominant in NiTi SMA subjected to plastic deformation at 800 °C, while it is unclear that whether CDRX is able to arise since the experimental evidence is insufficient in the present work.

It can be generally accepted that during DDRX of NiTi SMA, there is a competition between hardening mechanism due to dislocation storage and softening mechanism due to dislocation elimination. The competition mechanism is described as follows. When NiTi SMA is subjected to plastic deformation, the dislocation density increases with increasing plastic strain, and consequently the increase of the dislocation density leads to the occurrence of hardening mechanism. Simultaneously, the increasing dislocation density provides a driving force for the nucleation of the dynamic recrystallized grains, and thus the formation of the dynamic recrystallized grains result in the decrease of the dislocation density [11,20]. In the meantime, the DRV process is relatively slow, so the dislocation density is able to achieve a sufficiently high value to promote the nucleation of new recrystallized grains during plastic deformation. In general, the new recrystallized grains are nucleated preferentially at the grain boundaries, especially at the triple-junction of grain boundaries. The phenomenon is attributed to the fact that the dislocation density exhibits a higher value at the grain boundaries due to the pile-up of dislocations. However, according to the aforementioned results, it seems that the recrystallized grains are able to be nucleated in the grain interior. In general, NiTi SMA is in a three-dimension compressive stress state when it is subjected to local canning compression. This shall lead to the occurrence of high plastic strain in the local region of the grain interior. As a consequence, local high plastic strain results in local high dislocation density, which provides a driving force for the nucleation of the recrystallized grains in the grain interior. Of course, the corresponding experiment evidence shall be performed in the future.

In order to better give an insight into the distinction between DDRX and CDRX and to deeply understand the role of the dislocation density in DRX of NiTi SMA, the dislocation can be divided into statistically stored dislocation (SSD) and GND. In general, SSD is inherently responsible for plastic flow based on crystallographic slip on the distinct slip planes. However, GND results from the inhomogeneous plastic deformation, which is responsible for accommodating a given strain gradient and preserving crystallographic lattice compatibility. When NiTi SMA is subjected to plastic deformation at high temperatures, the slip systems are activated and consequently plenty of SSDs pile up towards the grain boundary. A high density of dislocations at the grain boundary lays the foundation for the nucleation of the recrystallized grains during DDRX of NiTi SMA. SSDs can tangle with each other even in the grain interior, and thus a high density of dislocations is formed in the grain interior. As a consequence, it is possible for the recrystallized grains to be nucleated in the grain interior. It can be generally accepted that there is not a rigorous dividing line between SSD and GND. In the case of CDRX, SSDs can be transformed into GNDs, which shall constitute the subgrain boundary. With the progression of plastic deformation, the subgrain boundary progressively absorbs GNDs and finally the new recrystallized grains are formed. It seems that GND plays a more important role in the formation of the new recrystallized grains during CDRX.

## 5. Conclusions

(1) In the case of 600 and 700 °C, DDRX and CDRX coexist in NiTi SMA. In the case of DDRX, the recrystallized grains are found to be nucleated at the grain boundary and even in the grain interior. The pile-up of SSDs lays the foundation for the nucleation of the recrystallized grains during DDRX of NiTi SMA. GND plays a significant role in the formation of new recrystallized grains during CDRX

of NiTi SMA. DDRX of NiTi SMA is attributed to a competition between hardening mechanism due to dislocation storage and softening mechanism due to dislocation elimination. In the case of CDRX, subgrain structures with low angle grain boundary are induced at the primary stage of plastic deformation and they are progressively transformed into the new grains with high angle grain boundaries after being subjected to large plastic strain. Furthermore, the dislocations are progressively absorbed during transformation from low angle grain boundaries to high angle grain boundaries.

(2) With increasing deformation temperature, fractions of the recrystallized grains and the substructures increase, whereas the fraction of the deformed grains decreases. Dynamic recrystallization has a significant influence on the texture evolution of NiTi SMA. In particular,  $\langle 110 \rangle$  texture of the as-rolled NiTi SMA is transformed into  $\langle 111 \rangle$  texture of the compressed NiTi SMA as a result of plastic deformation. Furthermore, the intensity of  $\langle 111 \rangle$  texture increases with increasing deformation temperature. It can be deduced that local canning compression causes NiTi SMA to be in a three-dimensional compressive stress state, which contributes to the occurrence of DRX. Furthermore, under the action of a three-dimensional compressive stress, the grains of NiTi SMA are preferentially orientated along with plastic deformation. As a consequence,  $\langle 111 \rangle$  texture is formed under the simultaneous action of DRX and compression deformation. The formation mechanism of  $\langle 111 \rangle$  texture shall be further investigated in the future.

**Acknowledgments:** The work was financially supported by National Natural Science Foundation of China (Nos. 51475101 and 51305091).

**Author Contributions:** Yanqiu Zhang performed EBSD analysis and wrote the manuscript; Shuyong Jiang supervised the research; Li Hu performed experiments and TEM analysis.

**Conflicts of Interest:** The authors declare no conflict of interest.

## References

1. Tadayyon, G.; Mazinani, M.; Guo, Y.; Zebarjad, S.M.; Tofail, S.A.M.; Biggs, M.J. The effect of annealing on the mechanical properties and microstructural evolution of Ti-rich NiTi shape memory alloy. *Mater. Sci. Eng. A* **2016**, *662*, 564–577. [[CrossRef](#)]
2. Shamsolhodaei, A.; Zarei-Hanzaki, A.; Ghambari, M.; Moemeni, S. The high temperature flow behavior modeling of NiTi shape memory alloy employing phenomenological and physical based constitutive models: A comparative study. *Intermetallics* **2014**, *53*, 140–149. [[CrossRef](#)]
3. Yeoma, J.T.; Kima, J.H.; Hong, J.K.; Kim, S.W.; Park, C.H.; Nam, T.H.; Lee, K.Y. Hot forging design of as-cast NiTi shape memory alloy. *Mater. Res. Bull.* **2014**, *58*, 234–238. [[CrossRef](#)]
4. Etaati, A.; Dehghani, K. A study on hot deformation behavior of Ni-42.5Ti-7.5Cu alloy. *Mater. Chem. Phys.* **2013**, *140*, 208–215. [[CrossRef](#)]
5. Morakabati, M.; Aboutalebi, M.; Kheirandish, S.; Karimi Taheri, A.; Abbasi, S.M. Hot tensile properties and microstructural evolution of as cast NiTi and NiTiCu shape memory alloys. *Mater. Des.* **2011**, *32*, 406–413.
6. Mirzadeh, H.; Parsa, M.H. Hot deformation and dynamic recrystallization of NiTi intermetallic compound. *J. Alloys Compd.* **2014**, *614*, 56–59. [[CrossRef](#)]
7. Basu, R.; Jain, L.; Maji, B.; Krishnan, M. Dynamic recrystallization in a Ni–Ti–Fe shape memory alloy: Effects on austenite–martensite phase transformation. *J. Alloys Compd.* **2015**, *639*, 94–101. [[CrossRef](#)]
8. Jiang, S.; Zhang, Y.; Zhao, Y. Dynamic recovery and dynamic recrystallization of NiTi shape memory alloy under hot compression deformation. *Trans. Nonferrous Met. Soc. China* **2013**, *23*, 140–147. [[CrossRef](#)]
9. Yin, X.Q.; Park, C.H.; Li, Y.F.; Ye, W.J.; Zuo, Y.T.; Lee, S.W.; Yeom, J.T.; Mi, X.J. Mechanism of continuous dynamic recrystallization in a 50Ti-47Ni-3Fe shape memory alloy during hot compressive deformation. *J. Alloys Compd.* **2017**, *693*, 426–431. [[CrossRef](#)]
10. Huang, K.; Logé, R.E. A review of dynamic recrystallization phenomena in metallic materials. *Mater. Des.* **2016**, *111*, 548–574. [[CrossRef](#)]
11. Sakai, T.; Belyakov, A.; Kaibyshev, R.; Miura, H.; Jonas, J.J. Dynamic and post-dynamic recrystallization under hot, cold and severe plastic deformation conditions. *Prog. Mater. Sci.* **2014**, *60*, 130–207. [[CrossRef](#)]
12. Xu, T.C.; Peng, X.D.; Qin, J.; Chen, Y.F.; Yang, Y.; Wei, G.B. Dynamic recrystallization behavior of Mg–Li–Al–Nd duplex alloy during hot compression. *J. Alloys Compd.* **2015**, *639*, 79–88. [[CrossRef](#)]

13. Liang, H.; Guo, H.; Ning, Y.; Peng, X.; Qin, C.; Shi, Z.; Nan, Y. Dynamic recrystallization behavior of Ti–5Al–5Mo–5V–1Cr–1Fe alloy. *Mater. Des.* **2014**, *63*, 798–804. [[CrossRef](#)]
14. Zhang, Z.; Yang, X.; Xiao, Z.; Jun, W.; Zhang, D.; Liu, C.; Sakai, T. Dynamic recrystallization behaviors of a Mg–4Y–2Nd–0.2Zn–0.5Zr alloy and the resultant mechanical properties after hot compression. *Mater. Des.* **2016**, *97*, 25–32. [[CrossRef](#)]
15. Li, Y.; Koizumi, Y.; Chiba, A. Dynamic recrystallization in biomedical Co–29Cr–6Mo–0.16N alloy with low stacking fault energy. *Mater. Sci. Eng. A* **2016**, *668*, 86–96. [[CrossRef](#)]
16. Wu, Y.; Zhang, X.; Deng, Y.; Tang, C.; Yang, L.; Zong, Y. Dynamic recrystallization mechanisms during hot compression of Mg–Gd–Y–Nd–Zr alloy. *Trans. Nonferr. Met. Soc. China* **2015**, *25*, 1831–1839. [[CrossRef](#)]
17. Zhang, B.; Liu, C.; Zhou, J.; Tao, C. Dynamic recrystallization of single-crystal nickel-based superalloy. *Trans. Nonferr. Met. Soc. China* **2014**, *24*, 1744–1749. [[CrossRef](#)]
18. Yamagata, H.; Ohuchida, Y.; Saito, N.; Otsuka, M. Nucleation of new grains during discontinuous dynamic recrystallization of 99.998 mass% Aluminum at 453 K. *Scr. Mater.* **2001**, *45*, 1055–1061. [[CrossRef](#)]
19. Yanushkevich, Z.; Belyakov, A.; Kaibyshev, R. Microstructural evolution of a 304-type austenitic stainless steel during rolling at temperatures of 773–1273 K. *Acta Mater.* **2015**, *82*, 244–254. [[CrossRef](#)]
20. Ouyang, D.L.; Fu, M.W.; Lu, S.Q. Study on the dynamic recrystallization behavior of Ti-alloy Ti–10V–2Fe–3V in  $\beta$  processing via experiment and simulation. *Mater. Sci. Eng. A* **2014**, *619*, 26–34. [[CrossRef](#)]



© 2017 by the authors. Licensee MDPI, Basel, Switzerland. This article is an open access article distributed under the terms and conditions of the Creative Commons Attribution (CC BY) license (<http://creativecommons.org/licenses/by/4.0/>).